CIMAC CONGRESS 25
ZURICH, MAY 19 – 23, 2025

2025 | 449

Machine learning-assisted spray pattern identification and prediction for liquid ammonia fuel

Fuel Injection & Gas Admission and Engine Components

Dawei Wu, University of Birmingham

Yifei Zhang, University of Birmingham
Wenjun Zhong, Jiangsu University
Zhixia He, Jiangsu University
Ebrahim Nadimi, University of Birmingham
Bihe Hu, University of Birmingham
Hongming Xu, University of Birmingham

DOI: https://doi.org/10.5281/zenodo.15195537

ABSTRACT

Liquid ammonia is interesting for the maritime industry due to its higher volumetric energy density and compatibility to existing large internal combustion engines (ICEs). Liquid ammonia injectors become the key enabling technology for existing ICEs to adopt a carbon-neutral alternative fuel. Ammonia has a high volatility, lower critical temperature, and higher critical pressure compared with most of the conventional liquid fuels. In advanced injection strategies of large modern ICEs, liquid ammonia sprays are prone to enter the vicinity of a critical point, the near metastable liquid region, and the transitional phases, which exhibit highly non-linear and unsteady behavior, potentially triggering combustion instabilities and engine failure.

The study incorporated both experimental tests on liquid ammonia sprays and machine learning-assisted spray pattern identification. In the experimental study, we applied both shadowgraph and Schlieren photography to examine the liquid ammonia spray patterns under different injection pressures (30 MPa, 50 MPa, and 65 MPa), six ambient pressures (0.1 MPa, 0.2 MPa, 0.4 MPa, 0.6 MPa, 0.8 MPa, and 1.2 MPa), and three nozzle orifice diameters (0.12 mm, 0.32 mm, and 0.52 mm) to obtain extensive data for further prediction analysis using machine learning. In the machine learning aspect, we constructed Backpropagation (BP), Genetic Algorithm-Backpropagation (GA-BP), and Particle Swarm Optimisation-Backpropagation (PSO-BP) neural networks based on liquid ammonia spray data under different conditions. These neural networks were trained to predict the penetration distance and other parameters of liquid ammonia spray across different phase change states (flash boiling, non-flash boiling, and transitional phases), and their predictive performances were evaluated and compared. Additionally, pseudo-color processing was used to analyse the flash boiling phenomenon and its influencing factors in liquid ammonia spray, and the predictive performance of the three neural network models under extrapolated experimental conditions was further examined.

The results indicate that the criterion of using superheat degree to determine the occurrence of flash boiling is not sufficient in the case of liquid ammonia. The nozzle diameter significantly influences the phase change in liquid ammonia spray, with the most pronounced effect. Among the neural networks, the PSO-BP model demonstrated the best performance in predicting the penetration distance across different phase change states. This study demonstrates the potential of BP neural networks, combined with optimisation algorithms, to improve the accuracy and generalisability of liquid ammonia spray penetration prediction models. By providing a detailed analysis of flash boiling conditions and their influencing factors, this research contributes to the development of more reliable and generalisable liquid ammonia spray models that can be applied to liquid ammonia injector development involving complex spray dynamics.

1 INTRODUCTION

The International Maritime Organization (IMO) has implemented stringent policies to reduce greenhouse gas emissions, further emphasizing the need for research and development of alternative fuels to replace conventional fossil fuels [1, 2]. The alternative fuels-based energy solutions need also need meet the growing energy demand with high efficiency and reliability. Ammonia stands out as a promising green fuel due to its carbon-free combustion and minimal nitrogen oxide emissions when the air-fuel ratio and combustion is optimized [3]. It offers practical storage options, requiring either 9 bar at room temperature or atmospheric pressure at -33°C, compared to hydrogen's stringent conditions of -253°C or 700 bar [4]. Moreover, existing efficient and sustainable ammonia production methods further bolster its viability as a future engine fuel [3, 5, 6].

Many studies have investigated the use of ammonia mixed with other fuels in engine experiments. For example, Reiter et al. [7] conducted experiments on dual-fuel engines using liquid ammonia and diesel, demonstrating the feasibility of ammonia as a diesel engine fuel at various engine speeds and loads. The researchers injected liquid ammonia through the intake manifold while injecting diesel directly into the cylinder. The study showed that by controlling the energy ratio of ammonia in the mixed fuel ($\leqslant$ 60%), NOx emissions could be reduced, and increasing the ammonia energy ratio could reduce CO2 emissions. Li et al. [8] compared dual-fuel modes of ammonia and diesel in a two-stroke marine diesel engine under low-pressure injection dual-fuel (LPDF) mode (intake manifold injection) and high-pressure injection dual-fuel (HPDF) mode (direct cylinder injection), finding that the ammonia substitution rate in HPDF mode could reach up to 97%, approximately 1.2 times that of LPDF mode. Moreover, HPDF mode also helps to reduce greenhouse gas emissions. Zhang et al. [9] studied the application of liquid ammonia HPDF technology in heavy-duty diesel engines. The researchers developed new injection strategies to improve fuel mixing efficiency and alter the distribution of ignition points within the cylinder. Compared to LPDF, HPDF mode not only maintains low greenhouse gas emissions but also effectively addresses NOx emissions at high energy ratios of ammonia, although partial ammonia unburned might occur. These studies confirm the potential of liquid ammonia as an alternative engine fuel and highlight the research trend towards using in-cylinder direct injection strategies for ammonia.

Studying the spray behavior of liquid ammonia is of significant importance for further optimizing internal combustion engines. During the injection process, liquid ammonia can undergo flash boiling under certain conditions. Flash boiling not only affects the spray morphology and droplet distribution but can also impact combustion efficiency and emission characteristics. The flash boiling phenomenon of liquid ammonia is influenced by various factors, including injection pressure, ambient temperature, nozzle geometry, and the physicochemical properties of ammonia. Many scholars have investigated the spray behavior of liquid ammonia from different perspectives.

Pele et al. [10] utilized a GDI injector for the first time to explore the flash boiling state of liquid ammonia. Their findings indicated that ambient density and ambient temperature significantly influence the development process of liquid ammonia spray. Cheng et al. [11] primarily investigated the effects of injection pressure and ambient pressure on flash boiling liquid ammonia spray through Schlieren imaging experiments. The study revealed that increasing injection pressure extends the penetration and spray area, while increasing ambient pressure enhances air resistance, resulting in the opposite effect. Additionally, due to the phase change characteristics of ammonia, the development of sprays at the same pressure ratio differs significantly between different phases. Li et al. [12] demonstrated that the degree of superheat, R_p=0.25 and R_p=0.5 are critical points distinguishing the initial flash boiling stage, transition stage, and flare-flashing stage of superheated ammonia spray. From the initial flash boiling stage to the critical point, the development of the ammonia spray penetration resembles that of diesel, whereas during the transition and flare-flashing stages, the penetration development varies due to bubble behavior. Fang et al. [13] also examined the performance of high-pressure liquid ammonia spray under flash and non-flash boiling conditions. They identified that under flash boiling conditions, the "spray resistance phenomenon" inhibits the spray tip velocity, and this phenomenon is highly correlated with R_p. Colson et al. [14] confirmed through experiments that R_p is a crucial parameter affecting the flash boiling state of liquid ammonia spray. R_p varies with changes in the nozzle length-to-diameter ratio (L/D). Moreover, increasing the nozzle diameter can induce more intense flash boiling phenomena. Liu et al. [15] showed through Schlieren imaging experiments that R_p=0.47 is the critical point distinguishing the flash boiling and transition stages of ammonia spray. The results indicated that as R_p increases, the penetration of ammonia spray in the flash boiling state also increases, while in the transition stage, the penetration decreases. Huang et al. [16] utilized large eddy simulation to study the effects of ambient pressure under flash boiling conditions

and both injection and ambient pressures under non-flash boiling conditions on the development of liquid ammonia spray. The simulation results were consistent with experimental results, confirming Cheng et al.'s findings [11], and comparing the radial expansion differences between flash and non-flash boiling sprays. He et al. [17] corroborated Cheng et al.'s conclusions [11] and further suggested that for non-flash boiling liquid ammonia spray, injection pressure does not significantly affect the development of spray penetration.

It is noteworthy that the superheat degree (R_p) has been proven in numerous studies to be a crucial parameter for identifying and distinguishing the flash boiling modes of liquid ammonia sprays. By adjusting the R_p value, the flash boiling state of liquid ammonia sprays can be effectively controlled, thereby influencing the spray penetration and morphology development. However, as demonstrated in the study by Colson et al. [14], the R_p value is influenced by other factors and is not constant. This also explains why different R_p values were obtained in the literature [12] and [15].

Despite the valuable insights provided by existing research into understanding the flash boiling state of liquid ammonia sprays, the extensive experimentation and analysis of the impact of each parameter are both time-consuming and complex. To more efficiently identify the spray patterns under different non-flash boiling and flash-boiling modes in highly volatile fuel sprays and predict relevant parameters, machine learning methods hold significant potential. Several studies have demonstrated the great prospects of machine learning in the field of volatile fuel sprays. Chang et al. [18] used three decision tree algorithms optimized by Tree-structured Parzen Estimator (TPE): Random Forest (RF), Gradient Boosting Regression Tree (GBRT), and Extreme Gradient Boosting (XGB) to predict and analyze the flash boiling spray characteristics of gasoline, with a particular focus on the prediction of spray tip penetration (STP) and downstream spray angle (SAdown). Results showed that the TPE-GBRT model had the highest accuracy in predicting STP, while the TPE-XGB model performed best in predicting SAdown. Hwang et al. [19] used a multilayer feedforward artificial neural network (ANN) to predict and analyze the spray characteristics of nine volatile fuels, including gasoline, under different flash boiling conditions, finding that the ANN model had high accuracy in predicting liquid penetration length and liquid volume fraction (LVF), especially under flash boiling conditions, surpassing existing computational fluid dynamics (CFD) models in prediction accuracy. Jeyaseelan et al. [20] applied a multilayer ANN algorithm to predict and analyze the spray angle and penetration length of cyclopentane under subcritical and trans-critical conditions. The study showed that the ANN model could accurately predict the spray characteristics of cyclopentane under different phase change conditions, performing exceptionally well under trans-critical conditions. Koukouvinis et al. [21] used an optimized ANN to predict and analyze the trans-critical spray characteristics of ECN Spray-A, with results showing that the ANN model had near-zero prediction errors for thermodynamic properties at high pressure (greater than 1 bar) and demonstrated high accuracy in predicting the temporal history of spray penetration length and spray distribution. Zhao et al. [22] employed a residual network (ResNet) and an optimized decision tree classifier (DTC) to identify and predict spray collapse modes for multi-component fuel mixtures. The study indicated that the ResNet model achieved over 99% accuracy in classifying spray collapse states, and the DTC model, combined with the modified superheat index (R_p), showed high precision in predicting spray collapse states.

These studies highlight the strong capability of machine learning in predicting parameters of volatile fuel sprays. The primary research focuses on using decision tree algorithms (such as Random Forest, Gradient Boosting Regression Tree, and Extreme Gradient Boosting) and ANN to predict parameters like spray tip penetration, spray angle, liquid penetration length, and liquid volume fraction. Additionally, deep learning models like ResNet have shown excellent performance in identifying spray collapse modes.

Research on liquid ammonia sprays is crucial for the development of HPDF engines. While existing spray experimental studies provide valuable data, they still fall short in terms of efficiency to support fast investigation and prototyping of new liquid ammonia injectors. Machine learning-assisted parameter prediction and pattern recognition can significantly improve this process's efficiency and accuracy. However, machine learning algorithms have not been widely applied to liquid ammonia spray research, representing a clear research gap. Although the superheat degree (R_p) can be used to identify and distinguish the flash boiling state of liquid ammonia, predicting the penetration of liquid ammonia directly through other input parameters (such as injection pressure, ambient pressure, and fuel temperature) is more comprehensive while using machine learning methods.

This study, based on experimental data from a previous work on liquid ammonia spray study, uses three neural networks—BP, GA-BP, and PSO-

BP—to predict the penetration of liquid ammonia under different non-flash boiling and flash-boiling states. Furthermore, the study attempts predictions for extrapolated experimental conditions (such as prediction of spray penetration under extreme high pressure which was not in the training dataset). This research aims to promote the application of liquid ammonia as a clean fuel in engine technology and provide a new perspective for predicting complex volatile fuel spray behaviors using machine learning techniques.

2 METHODOLOGY

2.1 The experimental rig for macroscopic spray visualization

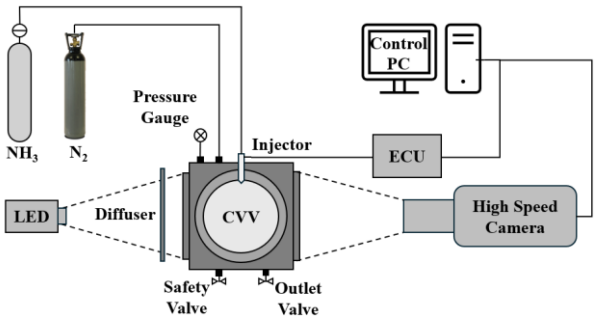

Figure 1. The schematic diagram of DBI system.

Figure 2. Diesel injector used in the experiment.

Figure 1 shows a schematic diagram of the entire experimental setup and the optical path arrangement system, which does not depict the actual layout of the experimental apparatus. Figure 2 shows the injector used in the liquid ammonia experiments, which is a diesel injector manufactured by Liaoning Xinfeng in China. The experimental setup mainly comprises a Diffuse Back Illumination (DBI) optical system, a high-pressure constant volume vessel (CVV), a control system, and a liquid ammonia injection system. The CVV features a window diameter of 80 mm, with its internal pressure supplied by a high-pressure nitrogen gas cylinder. A Fastcam SA-Z CMOS high-speed camera was employed in the experiments. The camera's recording resolution was set at 768 × 368 pixels, achieving a frame rate of 60,000 frames per second (fps) and a pixel scale ratio of 9.6 pixels/mm.

2.2 Fuel and experimental conditions

Liquid ammonia's density and viscosity vary with temperature and pressure are depicted in Figure 3. The experimental conditions encompassed a range of injection pressures, ambient pressures, and nozzle diameters. Specifically, there were three injection pressures (30 MPa, 50 MPa, and 65 MPa), six ambient pressures (0.1 MPa, 0.2 MPa, 0.4 MPa, 0.6 MPa, 0.8 MPa, and 1.2 MPa), and three nozzle orifice diameters (0.12 mm, 0.32 mm, and 0.52 mm) tested.

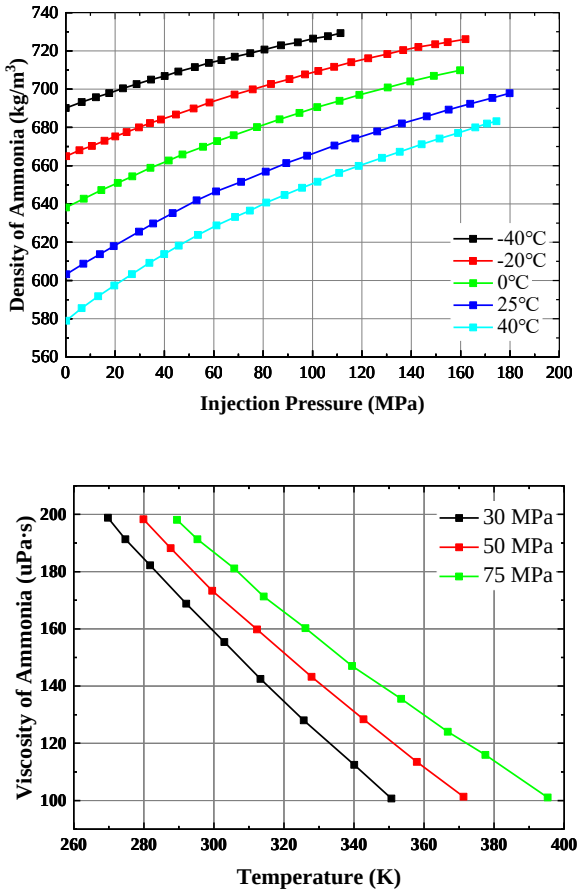

Figure 3. Density and viscosity of liquid ammonia as a function of temperature and pressure.

Table 1. Experimental conditions

Ambient pressure (MPa)	Injection pressure (MPa)	Nozzle Diameter (mm)	Injection duration (us)	Fuel temperature (K)	Ambient temperature (K)
0.1	30, 50, 65	0.12, 0.32, 0.52	2200	291	291
0.2	30	0.32			
0.4					
0.6					
0.8					
1.2	30, 50, 65	0.12, 0.32, 0.52			

Only the nozzle with a 0.32 mm orifice was subjected to all ambient pressure conditions during the experiments. Both the ambient temperature within the CVV and the fuel temperature were maintained at 18 °C throughout the experiments. All experimental conditions are detailed in Table 1. Each condition was repeated five times in the experimental study.

2.3 Image processing

The spray penetration for liquid ammonia spray is based on binary images obtained through image processing. The spray penetration is defined as the maximum pixel distance from the nozzle exit to the spray tip (Figure 4).

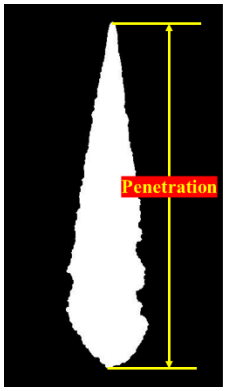

Figure 4. Density and viscosity of liquid ammonia as a function of temperature and pressure.

The selective raw spray images are provided in Appendix, Figure A1. The figure included the spray images under the conditions which were not presented in the existing literature [23].

2.4 BP neural networks for spray penetration prediction

Artificial Neural Networks (ANNs) represent a pivotal class within machine learning, capable of learning and improving from input "experiences" to become instrumental in data classification and prediction tasks. In this paper, BP neural network and its optimisation methods using different algorithms will be used for liquid ammonia spray penetration prediction. In Figure 5, it shows that the BP neural network, a variant of the feedforward neural network, employs the backpropagation algorithm to calculate the discrepancy between the network's output and the target output. This discrepancy is then propagated backwards through the network, allowing for the computation of each weight's (w_{ij}) and bias's (a_j and b_k) contribution to the error and subsequently deriving gradients for each parameter. These gradients are used to update weights and biases via gradient descent, thereby refining the network's output to align with the target output more closely [24-27].

However, BP neural network does not prescribe a specific strategy for updating weights, leading to potential issues such as local minima, slow convergence, or overfitting within backpropagation neural networks [28-30]. In this study, we used the basic BP neural network as a benchmarking method which is a single-hidden-layer, single-output network structure. The training algorithm employed is the Levenberg-Marquardt (L-M) algorithm. To compare with the basic BP neural network, two optimisation algorithms, namely Genetic Algorithm (GA) and Particle Swarm Optimisation (PSO) were integrated to address the limitations of the benchmarking method and enhance the efficiency and effectiveness of the training process. The input nodes included the time of spray development, injection pressure, ambient pressure, ambient density, fuel temperature, fuel density, fuel viscosity, and nozzle diameter, totaling eight input nodes. There is only one output node, which corresponds to the spray penetration. A total of 1686 data sets were collected for this experiment. 70% of the data sets were used as the training set, while 30% were used as the validation set. The experimental conditions which were used for the prediction purpose were left outside both the training and validation sets unseen by the BP neural networks.

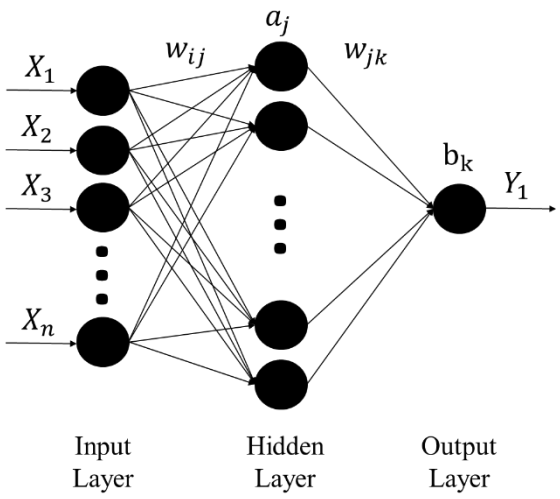

Figure 5. The structure of BP neural network.

2.4.1 Optimization algorithms

Figure 6 illustrates the primary workflow of GA, which is based on the principles of natural selection and genetics. Each potential solution (i.e., the set of weights and biases in a neural network) is encoded as a chromosome. Through operations such as selection, crossover, and mutation, GA explores and identifies optimal solutions [31]. In this study, the GA operations include roulette wheel selection, single-point crossover, and real-number mutation. Roulette wheel selection probabilistically

selects individuals based on their fitness values, while single-point crossover and real-number mutation generate new solutions by exchanging gene segments and finely adjusting gene values, respectively.

The flowchart of the PSO improved algorithm is depicted in Figure 7. PSO is grounded in swarm intelligence, mimics the social behaviors observed in flocks of birds or schools of fish. In PSO, each particle's position in the search space represents a potential solution, with its velocity dictating the direction and magnitude of exploration [32]. Particles adjust their positions and velocities based on their own best-known position and the global best position of the swarm, thereby progressively converging towards the optimal solution.

In existing literature, GA was studied for predicting spray penetration of conventional fuels [33, 34]. PSO has not yet been applied to improve neural networks to predict spray penetration, although it has been employed in other engineering parameter prediction studies. Some researchers have utilized PSO for predictive modeling and compared its performance with GA, demonstrating that PSO exhibits similar or even superior predictive potential [35-37].

The training of the BP neural networks involved 1,000 iterations in this study, with a learning rate set at 0.01 and a target minimum error of 1×10^{-5}. For the GA optimization, genes were encoded using real numbers, with each gene position constrained within the range [-3, 3]. The initial population size consisted of 30 individuals, with a maximum iteration limit of 50. The crossover and mutation probabilities were set at 0.8 and 0.2, respectively. The fitness value F for each individual was determined using the Root Mean Square Error (RMSE), calculated as:

$$F = RMSE = \sqrt{\frac{1}{n}\sum_{i=1}^{n}(y_i - Y_i)^2} \quad (1)$$

where n represents the number of samples, y_i is the predicted output from the neural network model, and Y_i is the actual experimental data.

For the PSO algorithm, the initial swarm size was set to 10 particles, with a maximum of 50 iterations. Each particle's position was confined within the range [-3, 3], and their velocities were limited to three times the range of each dimension. The cognitive and social learning factors were both fixed at 2, and the inertia weight was set at 0.9. The fitness value, like that in GA, was also evaluated using RMSE.

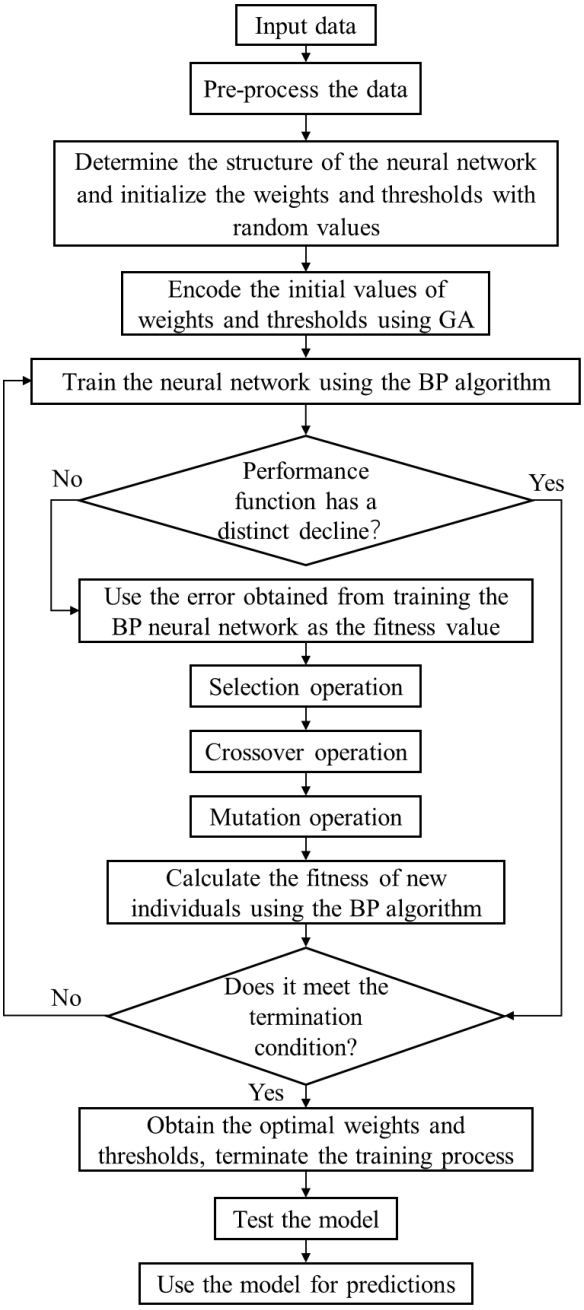

Figure 6. Flowchart of the GA-BP neural network.

2.4.2 Performance evaluation metrics

To evaluate performance of three neural networks (namely the baseline BP, the GA-BP, and the PSO-BP neural networks), a variety of metrics were used, including Coefficient of Determination (R^2, called as R-squared), Mean Absolute Percentage Error (MAPE), Mean Absolute Error (MAE), and RMSE. Each of these metrics reflects different aspects of a model's predictive accuracy.

R^2 measures the degree of correlation between the model's predicted values and the actual values, with its value ranging between [0, 1]. The R^2 value closer to 1 indicates stronger predictive power and

better fit of the model. The calculation formula for R^2 is:

$$R^2 = 1 - \frac{\sum_{i=1}^{n}(y_i - Y_i)^2}{\sum_{i=1}^{n}(Y_i - \bar{Y})^2} \quad (4)$$

where, $\bar{Y}$ is the mean of the actual values.

MAPE is the average of the absolute differences between the predicted and actual values, expressed as a percentage of the actual values. MAPE is particularly sensitive to outliers. A high MAPE value may indicate that, despite a good R^2 value suggesting a good fit, there are separate predictions that significantly deviate from the actual scenarios, which is unacceptable in many practical applications. The calculation formula for MAPE is:

$$MAPE = \frac{1}{n}\sum_{i=1}^{n}\frac{|y_i - Y_i|}{|y_i|} * 100\% \quad (5)$$

MAE is the average of the absolute differences between the predicted and actual values, providing a measure of the average level of errors.

$$MAE = \frac{1}{n}\sum_{i=1}^{n}(y_i - Y_i)^2 \quad (6)$$

Together with the fitness value, which is RMSE, four metrics are used in this study to compare different BP neural networks.

2.4.3 Selection of hidden layer node number

The selection of the number of nodes in the hidden layer of a neural network primarily involves two methods. The first method involves researchers presetting a range of node numbers and experimenting incrementally to determine the optimal number [38-40]. The second method employs empirical formulas derived from previous studies on hidden layer node selection [41, 42]. However, due to the influence of various factors such as the dimensionality of the input vector and the number of training examples, the optimal number of nodes obtained from the first method often lacks genericity [43, 44].

We discussed the various empirical formulas for hidden layer node selection methods including those proposed by Li et al. [45], Tamura and Tateishi [42], Xu and Chen [44], Shibata and Ikeda [43], and Hunter et al. [46] in a previous paper [47]. According to the previous study, Hunter et al.'s formula was chosen because it balances the trade-off between model complexity and computational efficiency. Therefore, the number of hidden layer nodes is 9.

$$N_h = N_i + 1 \quad (7)$$

where, N_h is the number of nodes in the hidden layer; N_i is the number of inputs / dimensions of the input vector.

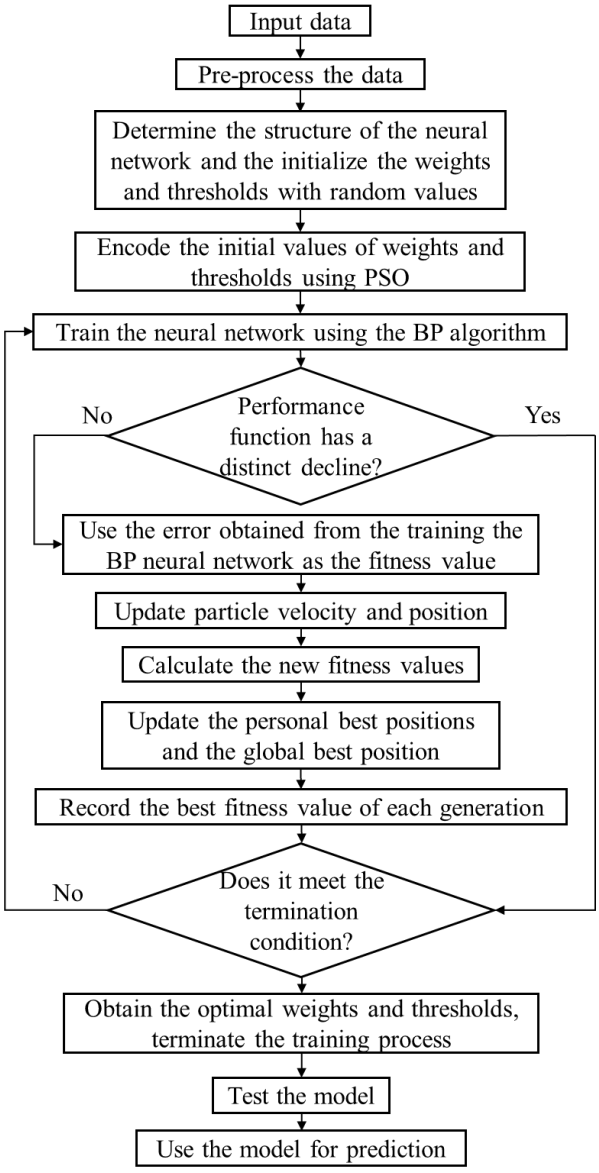

Figure 7. Flowchart of the PSO-BP neural network.

3 RESULTS AND DISCUSSION

3.1 Evaluation of different BP Neural Networks

3.1.1 Results of performance evaluation metrics

To evaluate the predictive capabilities of various neural network models for liquid ammonia spray penetration, a total of 1,686 experimental data points from liquid ammonia spray tests were used to train the BP, GA-BP, and PSO-BP neural networks respectively, each neural network for 30 times. Penetration data from a single experimental condition representative of three flash boiling

conditions were selected as the prediction set. For each trained model, key statistical metrics—including R^2, MAPE, RMSE, MAE, and execution time—were calculated and presented in Figure 8. Through the statistical analysis and comparison of these metrics, a comprehensive evaluation of three neural network models can be concluded.

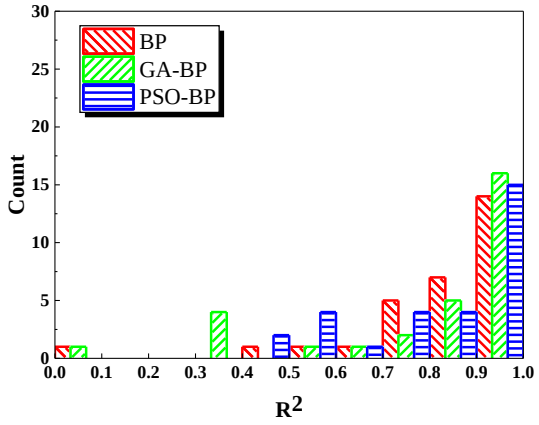

(a)

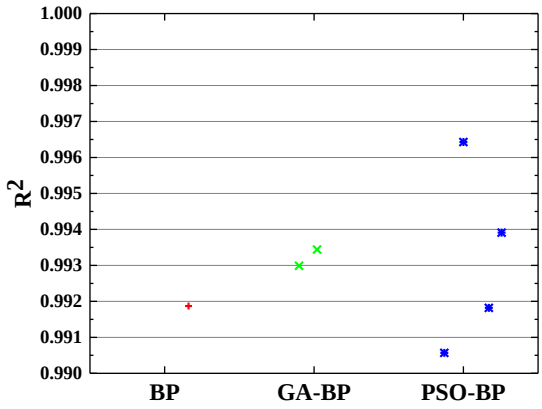

(b)

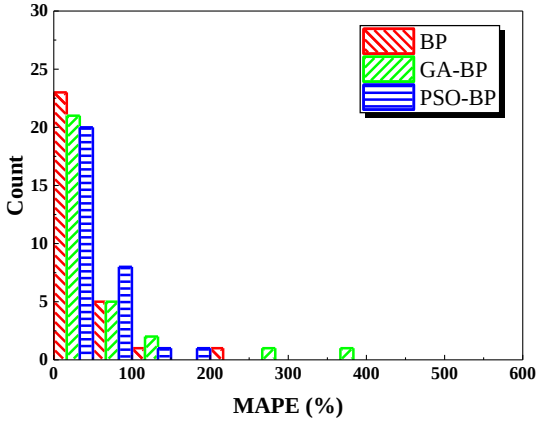

(c)

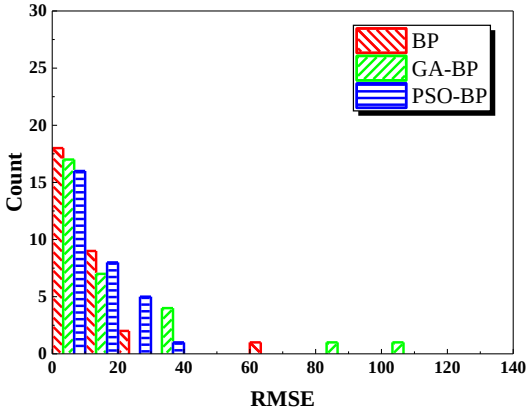

(d)

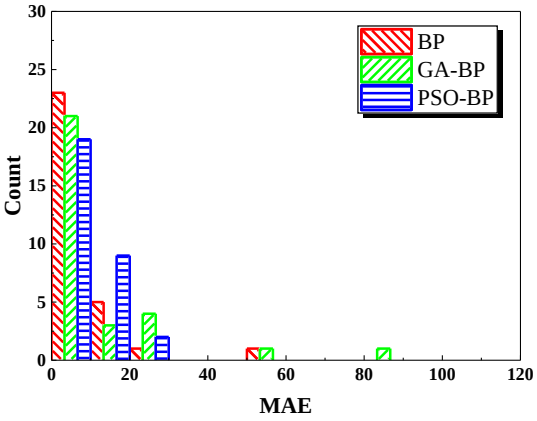

(e)

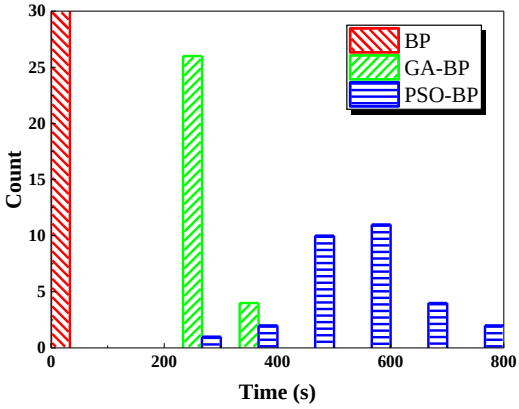

(f)

Figure 8. Comparison of R^2, MAPE, RMSE, MAE, and Execution Time for BP, GA-BP, and PSO-BP Neural Networks for spray penetration prediction.

In Figure 8(a), the overall R^2 distribution of the PSO-BP neural network outperforms the other models across all stages, with all predicted R^2 values exceeding 0.5. This indicates that the PSO-BP model demonstrates greater stability and robustness in capturing the variations in spray penetration. In contrast, the GA-BP and BP cases

exhibit a broader R^2 value distribution, reflecting their instability in handling the complexities of varying spray states. As shown in Figure 8 (b), in the high-accuracy range, the PSO-BP case shows a clear predictive advantage: 13.3% of its predictions fall within the R^2 range above 0.99, significantly higher than the 6.7% for the GA-BP and 3.3% for the BP baseline case. This result suggests that the PSO-BP neural network achieves overall superior prediction performance. The global searching capability of the PSO algorithm in optimizing initial neural network weights likely enhances its ability to avoid local minima, thereby improving the model's consistency and accuracy. Furthermore, the highest R^2 value achieved by the PSO-BP model is 0.99643, higher than the maximum values of 0.99344 for the GA-BP model and 0.99187 for the BP model.

Figure 8(c) illustrates the MAPE distribution for 30 prediction outcomes across the three neural network models, where the majority of MAPE values (more than 66.7%) fall within the 0 to 50 range. The PSO-BP model displays a concentrated distribution than the GA-BP. This concentration trend is likely influenced by two main factors: the impact of dataset segmentation and selection on model training and prediction accuracy, and differences in optimization strategies between the GA and PSO algorithms. The GA algorithm typically explores the solution space more quickly during the initial training stage, which may result in greater variations in outcomes. In contrast, the PSO algorithm demonstrates stronger global searching capabilities, leading to a significantly improved accuracy and consistency. Further analysis of Figures 8 (d) and (e) shows that the RMSE and MAE distributions closely align with the MAPE distribution, indicating consistent performance across multiple error metrics. This consistency is particularly pronounced in the PSO-BP neural network. It can be concluded that the PSO-BP model maintains strong predictive stability across different evaluation metrics.

The analysis of time efficiency in Figure 8 (f) shows that the BP neural network has the shortest training duration, typically completing within a few seconds, indicating a clear advantage in time efficiency. In contrast, the GA-BP model's training time generally stabilizes between 200 and 300 seconds, while the PSO-BP model exhibits the longest and most variable training times. This variability may be associated with the global optimization nature of the PSO algorithm, which requires longer iterative processes to achieve a global optimum, thereby increasing variability in training duration.

Incorporating optimization algorithms such as PSO and GA, enhances the model's capacity to detect and fit complex data patterns, with particularly notable improvements with the PSO-BP model. It consistently outperforms the BP and GA-BP models across all evaluation metrics, highlighting the effectiveness of global searching strategies in achieving higher predictive accuracy. However, the GA-BP model shows a relative deteriorated predictive performance, likely due to the increased non-linearity and complexity encountered due to a limited amount of data in the training set, although complicated physical phenomenon transition from non-flash to flash boiling of liquid ammonia sprays. It has relatively higher sensitivity to noise and outliers, which may be attributed to its reliance on diverse solution exploration and random search, which, while potentially beneficial for convergence, may also increase vulnerability to errors in noisy datasets. The standard BP model retains a clear advantage in time efficiency, despite lower overall accuracy. Together, these findings underscore the PSO-BP model's suitability for applications requiring high predictive accuracy and robustness.

3.1.2 Prediction results of liquid ammonia spray penetration

Based on the evaluation metrics results in the previous section, the highest-performing neural networks (determined by the highest R^2 value) were used for further analysis. The prediction results from the three selected models were subsequently compared with the experimental data from the prediction set. Notably, the experimental data in the prediction set, incorporated distinct spray conditions of liquid ammonia, encompassing flashing (R_p<0.25), non-flashing (R_p>1), and transitional phases (1>R_p>0.25).

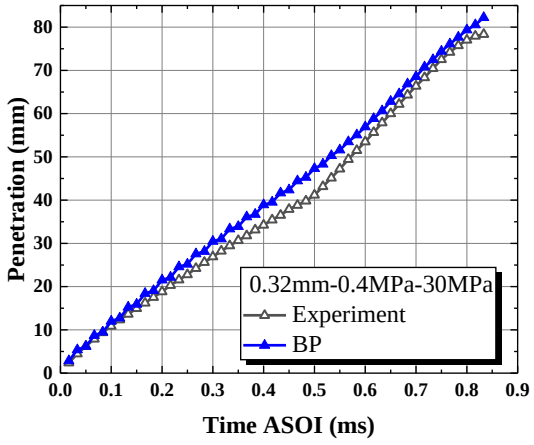

(a)

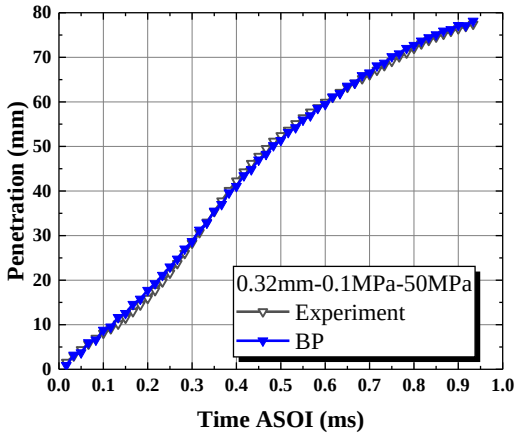
Penetration (mm)
Time ASOI (ms)
0.32mm-0.1MPa-50MPa
Experiment
BP

(b)

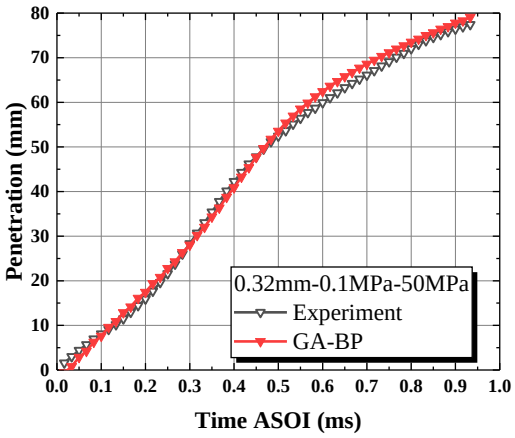
Penetration (mm)
Time ASOI (ms)
0.32mm-0.1MPa-50MPa
Experiment
GA-BP

(e)

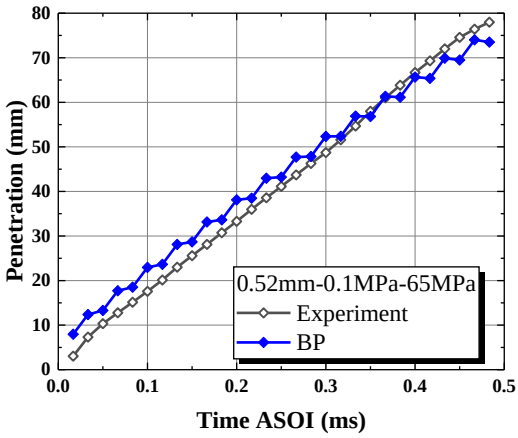
Penetration (mm)
Time ASOI (ms)
0.52mm-0.1MPa-65MPa
Experiment
BP

(c)

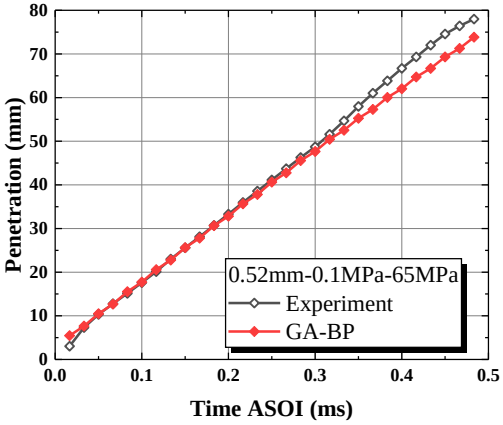
Penetration (mm)
Time ASOI (ms)
0.52mm-0.1MPa-65MPa
Experiment
GA-BP

(f)

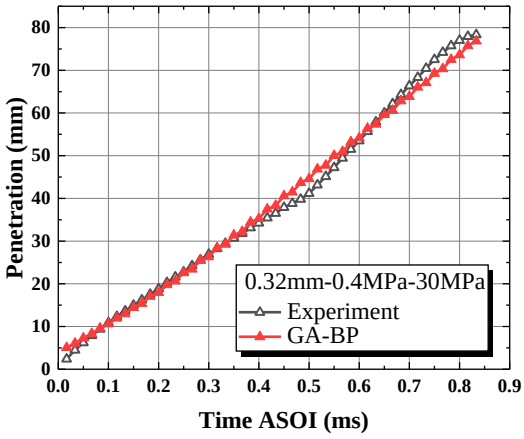
Penetration (mm)
Time ASOI (ms)
0.32mm-0.4MPa-30MPa
Experiment
GA-BP

(d)

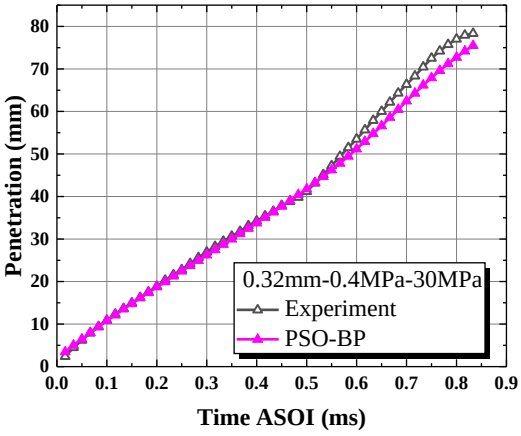
Penetration (mm)
Time ASOI (ms)
0.32mm-0.4MPa-30MPa
Experiment
PSO-BP

(g)

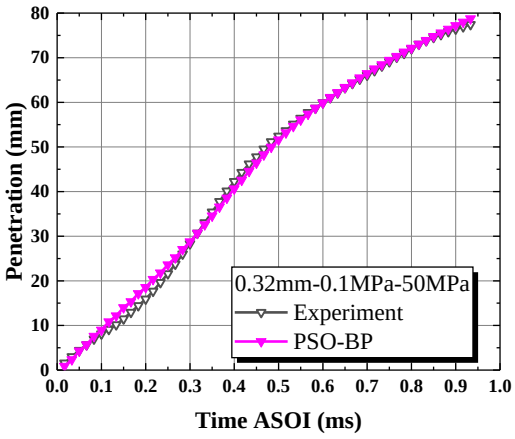

(h)

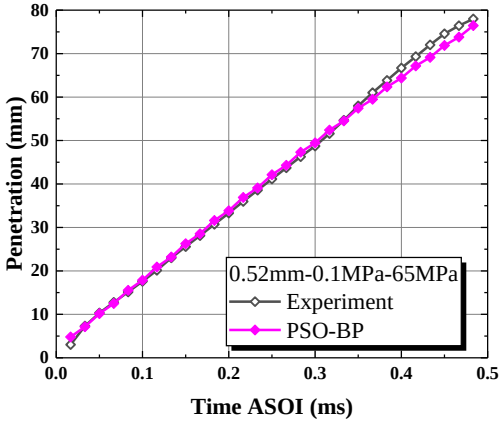

(i)

Figure 9. Comparison between the prediction results and the experimental data in the prediction set (0.32mm nozzle dia., 0.4 MPa background pressure, 30 MPa injection pressure/ 0.32mm nozzle dia., 0.1 MPa background pressure, 50 MPa injection pressure/ 0.52mm nozzle dia., 0.1 MPa background pressure, 65 MPa injection pressure)

Figure 9 (a-i) presents the predicted outcomes from the BP, GA-BP, and PSO-BP neural networks alongside the experimental results across various phase transition stages. In the non-flash boiling stage of liquid ammonia (0.32 mm-0.4 MPa-30 MPa), the BP model's prediction aligns with the experimental data during the initial and final stages of spray penetration; however, a deviation is observed during the middle segment of the spray development, indicating a limited ability to capture the complete penetration dynamics. The GA-BP model shows a close alignment with the experimental data and maintains high smoothness but ultimately shows linearity in some segments of the spray development, suggesting that the model lacks flexibility in capturing the more nuanced curvature of actual spray development. The PSO-BP model demonstrates both high smoothness and adaptability, closely tracking the experimental curve across all stages and capturing the continuous changes in penetration with minimal deviation. This suggests the PSO-BP model's robustness in handling steady, non-flashing spray behaviour.

During the transitional phase of liquid ammonia (0.32 mm-0.1 MPa-50 MPa), the BP model's prediction aligns well with experimental data in both values and trend, indicating a reasonable fit for this stage. The GA-BP model, while achieving a good fit during the middle stage of penetration, shows slight deviations in the initial and final stages, possibly due to its higher sensitivity to changing phase dynamics. The PSO-BP model, however, continues to demonstrate strong accuracy and smoothness, with its prediction curve closely aligning with the experimental data throughout the phase, underscoring its ability to adapt effectively to transitional phase changes.

In the flash boiling case of liquid ammonia (0.52 mm-0.1 MPa-65 MPa), the BP model's prediction displays a step-like pattern, which fails to capture the continuous spray development process observed in the experimental data and suggests limitations in predicting highly dynamic changes. The GA-BP model also shows significant deviation, especially in the final stage of spray penetration, possibly due to the increased non-linearity of the flash boiling spray. It is also possible that the limited number of flash-boiling experimental cases in the training set may also affect the accuracy of the spray penetration prediction. However, the PSO-BP neural network, with a high R^2 of 0.99643, demonstrates the best predictive performance across all stages, with a curve that remains smooth and highly consistent with the experimental data. This high degree of accuracy highlights the PSO-BP model's superior adaptability in capturing the complex, rapid transitions characteristic of flash boiling in liquid ammonia sprays.

Overall, the analysis shows that the PSO-BP model consistently delivers the most accurate and smooth predictions across non-flashing, transitional, and flash boiling stages, indicating its robustness in handling varying phase conditions. The BP and GA-BP neural networks, while effective in certain experimental cases, show limitations in fully capturing the complex transitions, particularly in highly dynamic phases like flash boiling.

3.2 Prediction of extrapolated experimental conditions

One important capability of neural networks, which is to achieve high accuracy of predicting extrapolated cases, is highly desired. For instance, the current liquid ammonia fuel supply system is limited to the highest pressure of 65 MPa, however,

it is important to understand the spray behavior at a higher injection pressure, more than 65 MPa. In this section, we regrouped the training, validation and prediction sets, and put all the cases of the injection pressure 65 MPa into the unseen prediction set. This will test three neural networks which one could have the best predictive performance for the extrapolated experimental conditions. If one of these models could reliably forecast spray penetrations in the extrapolated conditions in the prediction set, it potentially provides a practical solution to minimize the need for exhaustive physical spray experiments under extreme scenarios, such as very high injection pressures, significantly elevated ambient pressures and temperatures. This approach could significantly enhance experimental efficiency and reduce the costs associated with physical testing.

To accomplish this, the three datasets were restructured: data from conditions 0.32 mm-0.1 MPa-65 MPa and 0.32 mm-1.2 MPa-65 MPa were allocated to the prediction set, while the remaining data were divided into training and validation sets with a 7:3 ratio.

Figure 10 (a-f) illustrates the variations in prediction accuracy among the BP, GA-BP, and PSO-BP neural networks when applied to extrapolated experimental conditions. As shown in Figure 10 (a), an overall assessment of R^2 values across the 30 predictions shows that the BP model demonstrates relatively high stability, with 80% of its outcomes within the 0.9 to 1.0 range. The GA-BP model follows, achieving this range in 70% of its predictions, suggesting moderate consistency. In contrast, the PSO-BP model shows the least stability, with only about 50% of its predictions falling within this range, while the remaining results are more evenly distributed across the [0, 0.9] interval. This dispersion indicates that the PSO-BP model may struggle to maintain high prediction accuracy consistently under extrapolated conditions, which could be attributed to the increased complexity of modeling beyond the training data range.

3.2.1 Performance comparison of the three neural networks

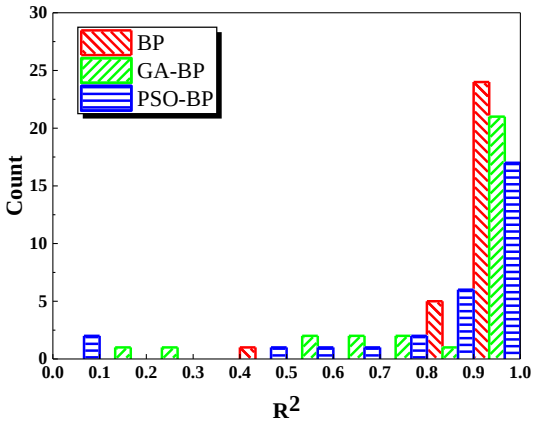

(a)

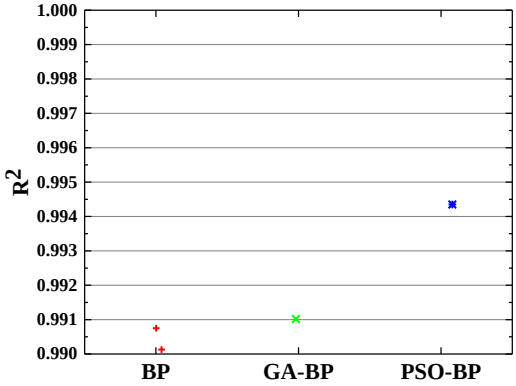

(b)

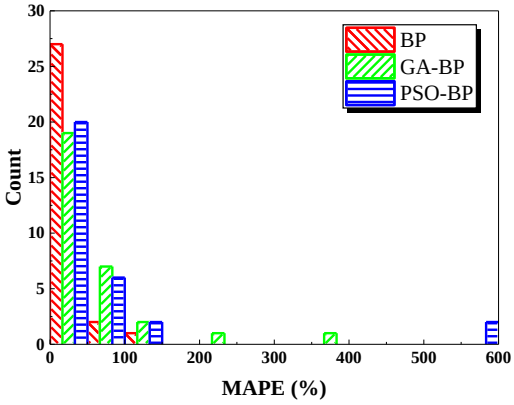

(c)

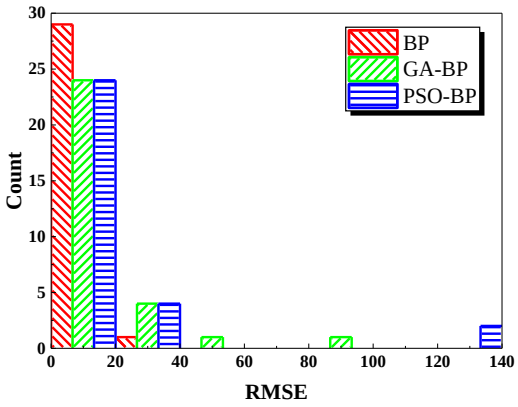

(d)

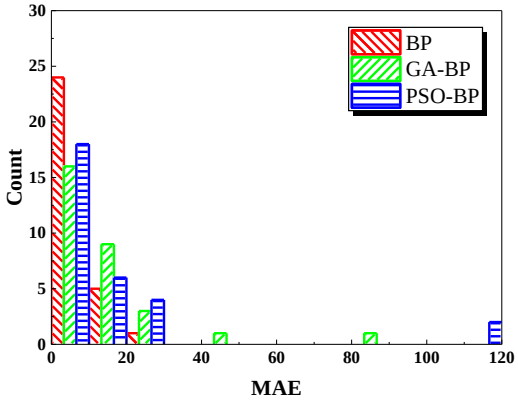

(e)

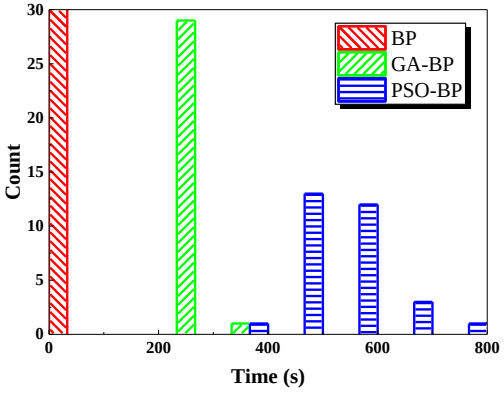

(f)

Figure 10. Comparison of R^2, MAPE, RMSE, MAE, and Execution Time for BP, GA-BP, and PSO-BP Models for Extrapolated Conditions.

When focusing on cases where $R^2 \geq 0.99$, as presented in Figure 10 (b), a clearer trend can be observed. The BP model meets this high-accuracy threshold in 6.7% of the cases, surpassing both the GA-BP and PSO-BP models, which achieve this threshold in only 3.3% of the cases. However, it is important to note that while the BP model maintains higher stability in reaching this threshold, its maximum R^2 does not exceed 0.991, indicating a limitation in achieving the highest accuracy levels. In contrast, the PSO-BP model, despite lower stability overall, achieves the highest R^2 of 0.99435, which is better than the GA-BP model's maximum result of 0.99102.

As illustrated in Figure 10 (c), an examination of the MAPE distribution across the 30 predictive outcomes under extrapolated experimental conditions shows that the BP neural network predominantly achieves MAPE values within the 0-50% range. This distribution indicates that the BP model, despite lacking optimization algorithms, has a lower tendency to produce extreme outliers compared to the GA-BP and PSO-BP models, whose MAPE values display greater variations. This suggests that while the BP model may yield more conservative predictions, it also exhibits more consistent accuracy, potentially due to its simpler structure, which may be less susceptible to divergence when extrapolating beyond the training data with the specific experimental parameter ranges.

Further analysis of Figures 10 (d) and (e) shows that the RMSE and MAE distributions closely align with those of MAPE across the models, reinforcing the consistency of error profiles for each network. Both GA-BP and PSO-BP models, although achieving high accuracy in certain instances, exhibit wider error ranges in these metrics, indicating greater sensitivity to novel, untrained data points in the extrapolated experimental conditions. This heightened variation could reflect the more complex nature of these models, which—despite algorithmic enhancements—may amplify deviations when faced with data outside the original training set.

In terms of time efficiency, as shown in Figure 10 (f), the standard BP model completes training within a remarkably short period, often under one second, underscoring its time efficiency advantage. The GA-BP model's training duration remains relatively stable, generally ranging from 200 to 300 seconds, suggesting moderate consistency in convergence. Conversely, the PSO-BP model demonstrates the longest and most variable training times, approximately two to three times longer than GA-BP. Although PSO is effective in quickly approaching the global optimum, its particle velocity update mechanism can lead to oscillations around the ultimate optimal solution, especially under extrapolated conditions where the search space may become more complex and non-linear. This oscillation delays convergence, highlighting a

trade-off between achieving high accuracy and maintaining time efficiency. Notably, the time efficiency performance of these three neural networks under extrapolated experimental conditions aligns with the trends observed in the last section.

In summary, the analysis of the prediction performance of BP, GA-BP, and PSO-BP neural networks for the extrapolated experimental conditions shows the strengths and limitations of each model. The BP model demonstrates relatively high stability, with consistent R^2 and MAPE values that reduce the occurrence of extreme outliers even without optimisation algorithms. Although the basic BP neural network offers rapid and stable training, it falls short in achieving high-precision fitting. The integration of optimisation algorithms such as PSO and GA enhances the model's capacity to search the solution space more thoroughly, thus improving the fitting accuracy for complex data (such as extrapolated experimental cases, with almost none knowledge from the training set). Nevertheless, these algorithms also introduce a higher risk of overfitting, as they tend to achieve the most precise solutions for training data, potentially generating noise rather than reasonable generic patterns applicable to physical experiments. Despite this risk, the addition of optimisation algorithms significantly increases the likelihood of achieving high-precision fitting. The GA-BP model shows improved accuracy with moderate consistency; however, its tendency for early convergence may limit adaptability under novel conditions. In contrast, while the PSO-BP model exhibits lower stability than the GA-BP neural network, it achieves the highest prediction accuracy demonstrating substantial potential. The PSO-BP model has the longest and most variable training time, due to the oscillatory convergence behaviour of its algorithm as it approaches the global optimum. Overall, the time efficiency trends of each model under extrapolated conditions align with the results observed in the last section, indicating that the processing duration of different neural network models is primarily determined by their optimisation algorithms and inherent model characteristics.

3.2.2 Best predictive neural networks for extrapolated experimental conditions

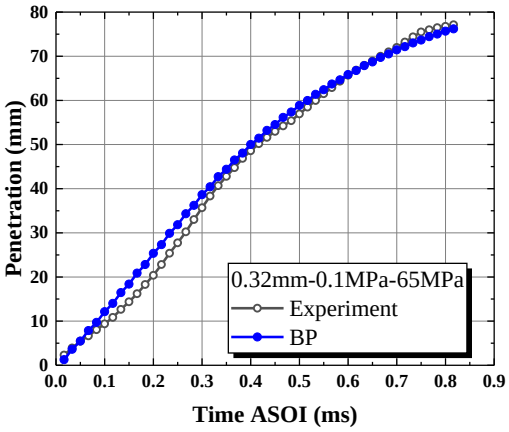

(a)

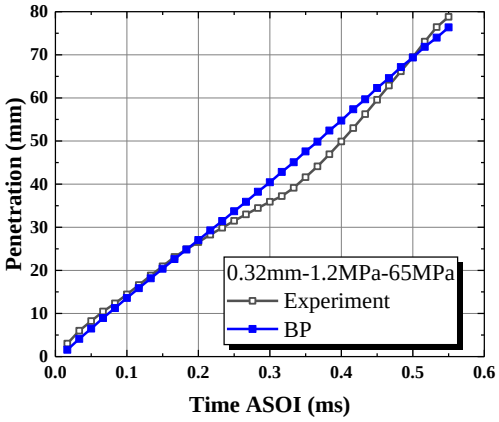

(b)

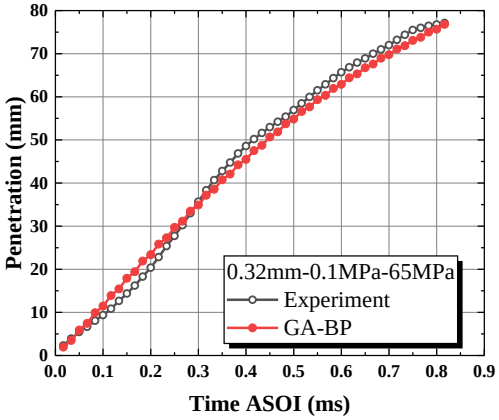

(c)

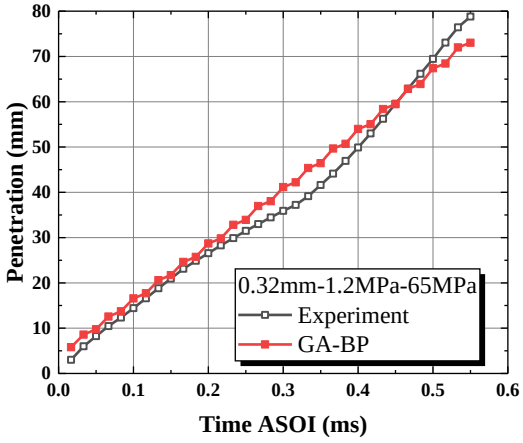

(d)

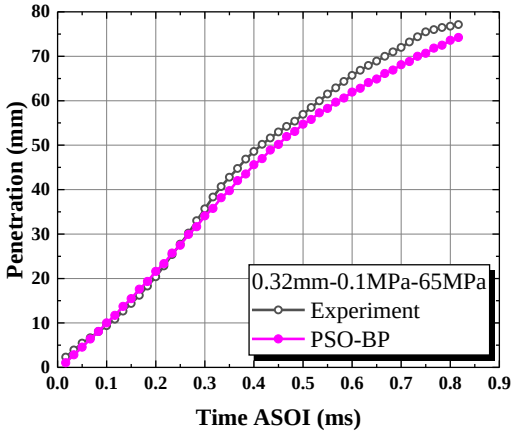

(e)

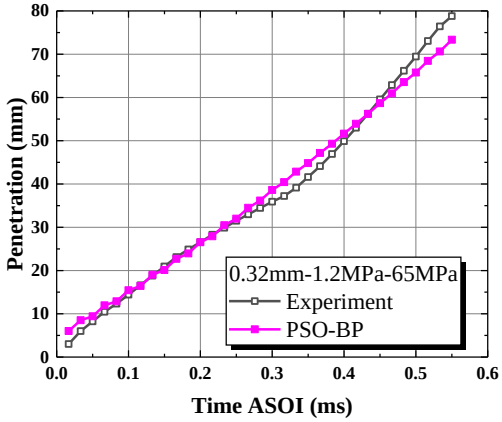

(f)

Figure 11. Best neural networks' prediction results for liquid ammonia spray penetration in the extrapolated experimental conditions (all the cases under high injection pressure of 65 MPa).

The highest-performing model from each neural network—BP (R^2 = 0.99075), GA-BP (R^2 = 0.99102), and PSO-BP (R^2 = 0.99435)—was selected to compare prediction performance under extrapolated experimental conditions. Figures 11 (a-f) present their time-varying predictions of liquid ammonia spray penetration in two extrapolated conditions.

Under the condition of 0.32 mm-0.1 MPa-65 MPa, the BP model's prediction closely matched the experimental data in the mid and late stages of the spray development but exhibited a clear deviation during the initial stages, where it struggled to capture the onset of penetration accurately. This limitation highlights BP's potential inadequacy in responding to rapid initial phase changes. The GA-BP model, despite a slightly higher R^2 value, displayed a similar trend, following the general pattern of spray development but missing subtle shifts in trajectory. The PSO-BP model, while not fully aligned with the experimental data, demonstrated superior adaptability especially the beginning stage.

For the more challenging conditions of 0.32 mm-1.2 MPa-65 MPa, all three models encountered difficulties. Although they captured the early-stage trends, none could reliably follow the turning points along the spray development curve, indicating the limitations of extrapolated predictions under the experimental conditions, unseen in the training set. The PSO-BP model's performance was the most promising, as its curve aligned more consistently with the experimental trajectory compared to BP and GA-BP; however, it still struggled with finer details. Meanwhile, the GA-BP model exhibited distinct step-like changes throughout its predictions. This "stair-step" pattern in GA-BP's predictions suggests sensitivity to fluctuations, potentially due to the GA algorithm's tendency to converge on local solutions rapidly, compromising prediction smoothness and accuracy in variable conditions.

In summary, while the PSO-BP model shows promising adaptability in handling some extrapolated conditions, with a higher overall R^2, the results highlight the intrinsic challenges to predict extrapolated conditions beyond the training data. This difficulty is particularly evident in phase-transition scenarios, where predictive models need heightened sensitivity to capture the complex, non-linear behaviour of liquid ammonia spray across its distinct flash-boiling states. A potential solution to this challenge could be that increasing number of interpolated testing conditions. More even representation within the training dataset, in another word, balanced proportions of data for distinctive non-flash boiling, transitional and flash-

boiling conditions, will assist to increase the models' ability to achieve enhanced accuracy and responsiveness in extrapolated experimental condition scenarios.

4 CONCLUSIONS

This study investigated using BP, GA-BP, and PSO-BP neural networks to develop predictive models for spray penetration of liquid ammonia injection. The results from three predictive models were examined using a group of performance evaluation metrics. Both interpolated and extrapolated experimental conditions were used to form the prediction dataset states to compare the effectiveness and accuracy of three models. The main conclusions are as follows:

1. By introducing evaluation metrics such as R^2, MAPE, RMSE, MAE, and execution time and comparing them from multiple perspectives, it was found that while the baseline BP neural network can complete training quickly and stably, its accuracy is compromised compared to the other two models integrated with optimization algorithms. The incorporation of optimization algorithms, such as PSO and GA enhances BP neural network's ability to handle complex problems. For extrapolated experimental conditions (high pressure conditions), the PSO model outperforms the other models in its accuracy.

2. Further comparison of all high-quality predictions ($R^2 > 0.99$) with experimental data showed that, although BP, GA-BP, and PSO-BP neural networks can all produce models with $R^2 > 0.99$, their prediction consistency with experimental data varies significantly. Apart from predictions for extrapolated experimental conditions, the PSO-BP model demonstrates a high accuracy which could successfully predict experimental spray development curves. More even representation within the training dataset may provide adequate information for the PSO-BP model to increase its accuracy and stability for predictions of extrapolated conditions.

5 DEFINITIONS, ACRONYMS, ABBREVIATIONS

ANN: Artificial neural network

BP: Backpropagation

CFD: Computational fluid dynamics

CVV: Constant-volume vessel

DBI: Diffused back-illumination

DTC: Decision tree classifier

HPDF: high-pressure injection dual-fuel

F: Fitness value

fps: Frame per second

GA: Genetic algorithm

GBRT: Gradient Boosting Regression Tree

L-M: Levenberg-Marquardt

LPDF: Low-pressure injection dual-fuel

LVF: Liquid volume fraction

MAE: Mean absolute error

MAPE: Mean absolute percentage error

MSE: Mean squared error

N_h**:** The number of nodes in the hidden layer

N_i**:** The number of inputs / dimensions of the input vector

PSO: Particle swarm optimisation

R^2**:** Coefficient of determination

RF: Random forest

R_p**:** The ratio of ambient pressure to saturation pressure

RMSE: Root mean squared error

Sa_{down}**:** Downstream spray angle

STP: Spray tip penetration

TPE: Tree-structured parzen estimator

XGB: Extreme gradient boosting

6 ACKNOWLEDGMENTS

This work was supported by EPSRC (Engineering and Physical Sciences Research Council, United Kingdom) (Grant numbers: EP/W016656/1, EP/Y024605/1).

7 APPENDIX

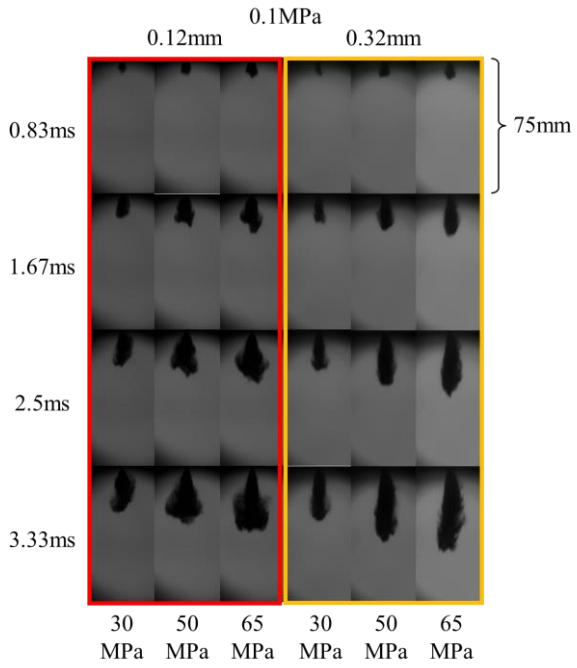

Figure A1. Images of liquid ammonia spray development over time under an ambient pressure of 0.1 MPa (nozzle diameter:0.12mm; injection pressure: 30MPa, 50MPa, 65MPa).

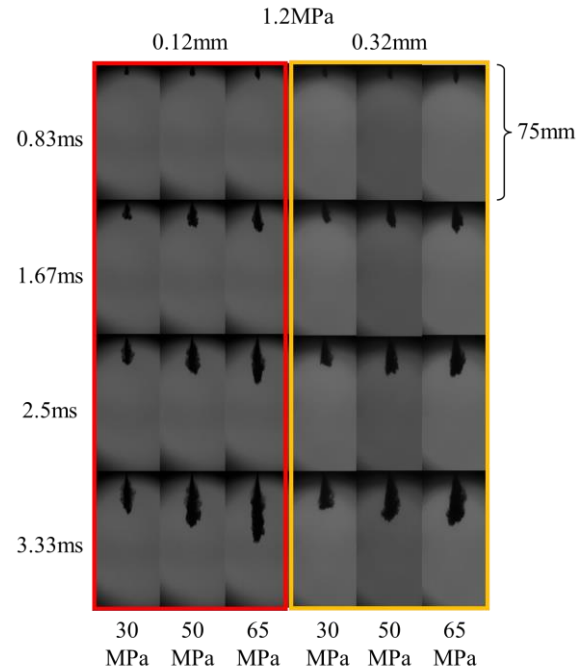

Figure A2. Images of liquid ammonia spray development over time under an ambient pressure of 1.2 MPa (nozzle diameter:0.12mm; injection pressure: 30MPa, 50MPa, 65MPa).

8 REFERENCES AND BIBLIOGRAPHY

[1] *The Paris Agreement*; Available from: https://unfccc.int/process-and-meetings/the-paris-agreement. [Accessed 27.05.2024 2024].

[2] *Net Zero by 2050*; May 2021. Available from: https://www.iea.org/reports/net-zero-by-2050. [Accessed 27.05.2024 2024].

[3] Zamfirescu C, Dincer I. 2009. Ammonia as a green fuel and hydrogen source for vehicular applications. *Fuel processing technology*, 90(5):729-37.

[4] Tornatore C, Marchitto L, Sabia P, De Joannon M. 2022. Ammonia as green fuel in internal combustion engines: State-of-the-art and future perspectives. *Frontiers in Mechanical Engineering*, 8:944201.

[5] Giddey S, Badwal S, Munnings C, Dolan M. 2017, Ammonia as a renewable energy transportation media. *ACS Sustainable Chemistry & Engineering*, 5(11):10231-9.

[6] Kurien C, Mittal M. 2023. Utilization of green ammonia as a hydrogen energy carrier for decarbonization in spark ignition engines. *International Journal of Hydrogen Energy.*

[7] Reiter AJ, Kong S-C. 2008. Demonstration of compression-ignition engine combustion using ammonia in reducing greenhouse gas emissions. *Energy & Fuels*, 22(5):2963-71.

[8Li T, Zhou X, Wang N, Wang X, Chen R, Li S, et al. 2022. A comparison between low-and high-pressure injection dual-fuel modes of diesel-pilot-ignition ammonia combustion engines. *Journal of the Energy Institute*, 102:362-73.

[9] Zhang Z, Di L, Shi L, Yang X, Cheng T, Shi C. 2024. Effect of liquid ammonia HPDI strategies on combustion characteristics and emission formation of ammonia-diesel dual-fuel heavy-duty engines. *Fuel*, 367:131450.

[10] Pelé R, Mounaïm-Rousselle C, Bréquigny P, Hespel C, Bellettre J. 2021. First study on ammonia spray characteristics with a current GDI engine injector. *Fuels*,2(3):253-71.

[11] Cheng Q, Ojanen K, Diao Y, Kaario O, Larmi M. 2022. Dynamics of the ammonia spray using high-speed schlieren imaging. *SAE Technical Papers*, 2022.

[12] Li S, Li T, Wang N, Zhou X, Chen R, Yi P. 2022. An investigation on near-field and far-field

characteristics of superheated ammonia spray. *Fuel*, 324:124683.

[13] Fang Y, Ma X, Zhang Y, Li Y, Zhang K, Jiang C, et al. 2023. Experimental investigation of high-pressure liquid ammonia injection under non-flash boiling and flash boiling conditions. *Energies*, 16(6):2843.

[14] Colson S, Yamashita H, Oku K, Somarathne KDKA, Kudo T, Hayakawa A, et al. 2023. Study on the effect of injection temperature and nozzle geometry on the flashing transition of liquid ammonia spray. *Fuel*, 348:128612.

[15] Liu X, Yao X, Wang Z, Tang C. 2023. Single hole ammonia spray macroscopic and microscopic characteristics at flare and transition flash boiling regions. *Applied Thermal Engineering*, 235:121443.

[16] Huang Z, Wang H, Luo K, Fan J. 2023. Large eddy simulation investigation of ammonia spray characteristics under flash and non-flash boiling conditions. *Applications in Energy and Combustion Science*, 16:100220.

[17] He H, Wu J, Wang L, Lou H, Li S, Huang L, et al. 2024. An Experimental Study on the Flash Boiling Characteristics of Liquid Ammonia Spray in a Constant Volume Chamber under High Injection Pressure. *Processes*,12(6):1076.

[18] Chang M, Park S. 2023. Predictions and analysis of flash boiling spray characteristics of gasoline direct injection injectors based on optimized machine learning algorithm. *Energy*, 262:125304.

[19] Hwang J, Lee P, Mun S, Karathanassis IK, Koukouvinis F, Tagliante F, et al. 2022. A new pathway for prediction of gasoline sprays using machine-learning algorithms. *SAE International Journal of Advances and Current Practices in Mobility*, 5(2022-01-0492):343-56.

[20] Jeyaseelan T, Son M, Sander T, Zigan L. 2023. Experimental and modeling analysis of the transient spray characteristics of cyclopentane at sub-and transcritical conditions using a machine learning approach. *Physics of Fluids*, 35(8).

[21] Koukouvinis P, Rodriguez C, Hwang J, Karathanassis I, Gavaises M, Pickett L. 2022. Machine Learning and transcritical sprays: A demonstration study of their potential in ECN Spray-A. *International Journal of Engine Research*, 23(9):1556-72.

[22] Zhao F, Zhou Z, Liu W, Hung DL. 2023. Data-driven detection and prediction of spray collapse characteristics for multi-component fuel mixtures. *Internal Combustion Engine Division Fall Technical Conference*, V001T03A3.

[23] Ma Y, Zhong W, Lai S, Chen J, Pachiannan T, Zhang L, et al. 2024. Experimental study on the flash boiling spray characteristics and jet fluctuation of high-pressure direct injection liquid ammonia. *Applied Thermal Engineering*, 257:124032.

[24] Rumelhart DE, Hinton GE, Williams RJ. 1986. Learning representations by back-propagating errors. *Nature*, 323(6088):533-6.

[25] Karazi S, Moradi M, Benyounis K. 2019. Statistical and numerical approaches for modelling and optimising laser micromachining process-Review. *Reference Module in Materials Science and Materials Engineering*.

[26] Ní Mhurchú J. 2008. Dead-end and crossflow microfiltration of yeast and bentonite suspensions: experimental and modelling studies incorporating the use of artificial neural networks. Dublin City University.

[27] Aydiner C, Demir I, Yildiz E. 2005. Modeling of flux decline in crossflow microfiltration using neural networks: the case of phosphate removal. Journal of membrane science, 248(1-2):53-62.

[28] Cui Z, Wang L, Li Q, Wang K. 2022. A comprehensive review on the state of charge estimation for lithium‐ion battery based on neural network. *International Journal of Energy Research*, 46(5):5423-40.

[29] Hosseinzadeh M, Ahmed OH, Ghafour MY, Safara F, Hama HK, Ali S, et al. 2021. A multiple multilayer perceptron neural network with an adaptive learning algorithm for thyroid disease diagnosis in the internet of medical things. The Journal of Supercomputing, 77:3616-37.

[30] Wang W, Xu Z, Weizhen Lu J. 2003. Three improved neural network models for air quality forecasting. *Engineering Computations*, 20(2):192-210.

[31] ROOIJ V. 1996. Neural network training using genetic algorithms. World Scientific Series on Machine Perception & Artificial Intelligence, 26.

[32] Mikki SM, Kishk AA. 2008. Particle swarm optimization: A physics-based approach. *Morgan & Claypool Publishers*.

[33] Taghavifar H, Khalilarya S, Jafarmadar S. 2014. Diesel engine spray characteristics prediction with hybridized artificial neural network optimized by genetic algorithm. *Energy*, 71:656-64.

[34] Weber J, Spiekermann P, Peters N. 2005. Model calibration for spray penetration and mixture formation in a high pressure fuel spray using a micro-genetic algorithm and optical data. *SAE transactions*, 1417-43.

[35] Liao J, Hu J, Yan F, Chen P, Zhu L, Zhou Q, et al. 2023. A comparative investigation of advanced machine learning methods for predicting transient emission characteristic of diesel engine. *Fuel*, 350:128767.

[36] Benteşen Yakut Y. 2024. Optimization of Proportional–Integral (PI) and Fractional-Order Proportional–Integral (FOPI) Parameters Using Particle Swarm Optimization/Genetic Algorithm (PSO/GA) in a DC/DC Converter for Improving the Performance of Proton-Exchange Membrane Fuel Cells. *Energies*, 17(4):890.

[37] Fang C, Liu F, Yang J, Wang S, Liu C, Mu Y, et al. 2023. Predicting the Sauter mean diameter of swirl cup airblast fuel injector based on backpropagation (BP) neural network model. *ACS omega*, 8(43):40162-73.

[38] Liu Y, Tian J, Song Z, Li F, Zhou W, Lin Q. 2022. Spray characteristics of diesel, biodiesel, polyoxymethylene dimethyl ethers blends and prediction of spray tip penetration using artificial neural network. *Physics of Fluids*, 34(1).

[39] Tian J, Liu Y, Bi H, Li F, Bao L, Han K, et al. 2022. Experimental study on the spray characteristics of octanol diesel and prediction of spray tip penetration by ANN model. *Energy*, 239:121920.

[40] Zhang Z, Wei S, Zhang S, Ni S. 2024. Study of RP-3/n-butanol fuel spray characteristics and ANN prediction of spray tip penetration. *Energy*, 292:130515.

[41] Sheela KG, Deepa SN. 2013. Review on methods to fix number of hidden neurons in neural networks. *Mathematical problems in engineering*, 2013.

[42] Tamura Si, Tateishi M. 1997. Capabilities of a four-layered feedforward neural network: four layers versus three. *IEEE Transactions on Neural Networks*, 8(2):251-5.

[43] Shibata K, Ikeda Y. 2009. Effect of number of hidden neurons on learning in large-scale layered neural networks. *2009 ICCAS-SICE. IEEE*; 2009:5008-13.

[44] Xu S, Chen L. 2008. A novel approach for determining the optimal number of hidden layer neurons for FNN's and its application in data mining. 2008.

[45] Li J-Y, Chow TW, Yu Y-L. 1995. The estimation theory and optimization algorithm for the number of hidden units in the higher-order feedforward neural network. Proceedings of ICNN'95-International Conference on Neural Networks. *3. IEEE*, 1229-33.

[46] Hunter D, Yu H, Pukish III MS, Kolbusz J, Wilamowski BM. 2012. Selection of proper neural network sizes and architectures—A comparative study. *IEEE Transactions on Industrial Informatics*, 8(2):228-40.

[47] Zhang Y, Zhang G, Wu D, Wang Q, Nadimi E, Shi P, et al. 2024. Parameter sensitivity analysis for diesel spray penetration prediction based on GA-BP neural network. *Energy and AI*, 18:100443.